

# A perturbative determination of $O(a)$ boundary improvement coefficients for the Schrödinger Functional coupling at 1-loop with improved gauge actions

Shinji Takeda, Sinya Aoki and Kiyotomo Ide  
 Institute of Physics, University of Tsukuba  
 Ibaraki 305-8571, Japan

May 10, 2018

## Abstract

We determine  $O(a)$  boundary improvement coefficients up to 1-loop level for the Schrödinger Functional coupling with improved gauge actions including plaquette and rectangle loops. These coefficients are required to implement 1-loop  $O(a)$  improvement in full QCD simulations for the coupling with the improved gauge actions. To this order, lattice artifacts of step scaling function for each improved gauge action are also investigated. In addition, passing through the SF scheme, we estimate the ratio of  $\Lambda$ -parameters between the improved gauge actions and the plaquette action more accurately.

## 1 Introduction

The  $\overline{\text{MS}}$ -scheme now becomes the standard renormalization scheme for the definition of the strong coupling constant. The measured coupling constant  $\alpha_s$  in some experiment at relatively high energy is converted to  $\alpha_{\overline{\text{MS}}}$  at some representative scale by perturbation theory. The current world average of such estimates gives  $\alpha_{\overline{\text{MS}}}(m_Z = 91.19\text{GeV}) \approx 0.11$ . Lattice QCD calculations, on the other hand, have a potential ability to determine the the strong coupling constant from the experimental inputs at low (hadronic) energy scale. In order to compare the coupling constant obtained at low energy by the lattice calculations with  $\alpha_{\overline{\text{MS}}}$  obtained at high energy, the Schrödinger Functional scheme has been proposed by the ALPHA collaboration [1], and the scheme is shown to be successful. At present, the results on the running coupling constant of two massless flavor QCD are reported [2, 3].

In the real world there are three light quarks. QCD simulations including three dynamical quark effects are thus required to understand the low energy QCD dynamics. Our ultimate goal is to estimate  $\alpha_{\overline{\text{MS}}}$  from  $N_f = 3$  QCD simulations. Recently, CP-PACS/JLQCD collaborations have started the  $N_f = 3$  QCD simulation employing an exact fermion algorithm developed for odd number of quark flavors [4, 5, 6]. In particular, noteworthy results have been obtained in [5]: There exists strong lattice artifacts associated with the phase transition in the  $N_f = 3$  QCD

simulation with the combination of the plaquette gauge action and  $O(a)$  improved Wilson quark action, while such lattice artifacts are absent for the renormalization group (RG) improved gauge action. Hence, the collaborations have decided to adopt the combination of the RG improved gauge action and  $O(a)$  improved Wilson quark action for the  $N_f = 3$  QCD simulations to obtain  $\alpha_{\overline{\text{MS}}}$ .

As a first step of our program, we study a Schrödinger Functional coupling with improved gauge actions in perturbation theory. In particular we perturbatively calculate the  $O(a)$  boundary improvement coefficients at 1-loop level with improved gauge actions for the pure  $SU(3)$  gauge theory. Combining this with the 1-loop results for the fermionic sector [7], we determine the  $O(a)$  boundary improvement coefficients at 1-loop, which can be used for the dynamical quark simulations in the future.

The rest of this paper is organized as follows. In Sect 2, after a brief reminder of the Schrödinger Functional scheme and its extension to improved gauge actions, we specify an action used for latter calculations, and discuss the  $O(a)$  boundary counterterm. In Sect 3 the Schrödinger Functional coupling constant is defined and formula for a determination of the  $O(a)$  boundary improvement coefficients are given. The 1-loop computation is outlined in Sect 4, and the results of the  $O(a)$  boundary improvement coefficients are summarized in Sect 5. Our conclusion is given in the last section, together with a discussion on the lattice artifact of the step scaling function.

## 2 Preliminaries

### 2.1 Schrödinger Functional

It has been shown by ALPHA collaboration that the Schrödinger Functional (SF) scheme is a powerful tool to probe energy evolutions of some physical quantities and to compute improvement coefficients as well as renormalization constants. In the SF scheme, the theory is defined on a finite box of size  $L^3 \times T$  with periodic boundary conditions in the spatial directions and Dirichlet boundary conditions in the time direction. In the pure  $SU(3)$  gauge theory with Wilson plaquette action  $S[U]$ , the partition function in the SF scheme (in the case that  $T = L$ ) is given by

$$\mathcal{Z} = \int D[U] e^{-S[U]}, \quad (2.1)$$

where link variables  $U(\mu, x)$  for gauge fields satisfy boundary conditions

$$U(x, k)|_{x_0=0} = \exp\{aC\}, \quad U(x, k)|_{x_0=L} = \exp\{aC'\}. \quad (2.2)$$

Here  $a$  is lattice spacing, and  $C, C'$  are diagonal traceless matrices, which depend on background field parameters  $\eta$  and  $\nu$  [8]. It is shown[1] that the minimum of  $S[U]$  is given by the lattice background field  $U(x, \mu) = V(x, \mu)$ , where

$$V(x, 0) = 1, \quad V(x, k) = V(x_0), \quad (2.3)$$

with

$$V(x_0) = \exp\{ab(x_0)\}, \quad (2.4)$$

$$b(x_0) = \frac{1}{L}[(L - x_0)C + x_0C']. \quad (2.5)$$

This background field represents a constant electric field.

An extension of the SF scheme to improved gauge actions was first considered by Klassen [9]. The transfer matrix construction [10] was adopted in the discussion. In this formulation, Each boundary consists of two time slices, to achieved the tree-level  $O(a^2)$  improvement.

In this paper, however, we adopt the formulation proposed by Aoki, Frezzotti and Weisz [11], where each boundary consists of only one time slice and the tree-level  $O(a)$  improvement is achieved: Dynamical variables to be integrated over are independent on the form of the action, plaquette or improved ones, and are given by the spatial link variables  $U(k, x)$  with  $x_0 = a, \dots, L - a$  and temporal link variables  $U(0, x)$  with  $x_0 = 0, \dots, L - a$  on a cylinder with volume  $L^3 \times L$ . This formulation is implemented more easily in numerical simulations.

The background field in eq.(2.3) gives the local minimum of the theory in both cases [9] and [11]. It has not been theoretically proved, however, that eq.(2.3) is the absolute minimum for the improved gauge actions. This is checked only numerically [9].

## 2.2 Gauge action

Our improved action includes plaquette and rectangle loops, and is given by

$$S_{\text{imp}}[U] = \frac{1}{g_0^2} \sum_{\mathcal{C} \in \mathcal{S}_0} W_0(\mathcal{C}, g_0^2) 2\mathcal{L}(\mathcal{C}) + \frac{1}{g_0^2} \sum_{\mathcal{C} \in \mathcal{S}_1} W_1(\mathcal{C}, g_0^2) 2\mathcal{L}(\mathcal{C}), \quad (2.6)$$

with

$$\mathcal{L}(\mathcal{C}) = \text{ReTr}[I - U(\mathcal{C})], \quad (2.7)$$

where  $U(\mathcal{C})$  is the ordered product of the link variables along loop  $\mathcal{C}$  contained in the set  $\mathcal{S}_0$ (plaquette) or  $\mathcal{S}_1$ (rectangular).  $\mathcal{S}_0$  and  $\mathcal{S}_1$  consist of all loops of the given shape which can be drawn on the cylindrical lattice with volume  $L^3 \times L$ . The loops involve only the “dynamical links” in the sense specified above, and spatial links on the boundaries at  $x_0 = 0$  and  $x_0 = L$ . In particular, rectangles protruding from the boundary of the cylinder are not included.

One has to choose appropriate boundary weights to achieve the 1-loop level  $O(a)$  improvement for observables involving derivative with respect to the boundary. Among various choices to achieve this, ours is given as follows.

$$W_0(\mathcal{C}, g_0^2) = \begin{cases} c_s(g_0^2) & \text{for } \mathcal{C} \in P_s : \text{Set of plaquettes that lie on one of} \\ & \text{the boundaries,} \\ c_0 c_t^P(g_0^2) & \text{for } \mathcal{C} \in P_t : \text{Set of plaquettes that just touch one} \\ & \text{of the boundaries,} \\ c_0 & \text{for } \mathcal{C} \in P_{\text{other}} : \text{otherwise,} \end{cases} \quad (2.8)$$

$$W_1(\mathcal{C}, g_0^2) = \begin{cases} 0 & \text{for } \mathcal{C} \in R_s : \text{Set of rectangles that lie completely} \\ & \text{on one of the boundaries,} \\ c_1 c_t^R(g_0^2) & \text{for } \mathcal{C} \in R_t^2 : \text{Set of rectangles that have exactly 2} \\ & \text{links on a boundary,} \\ c_1 & \text{for } \mathcal{C} \in R_{\text{other}} : \text{otherwise,} \end{cases} \quad (2.9)$$

with

$$c_0 c_t^P(g_0^2) = c_0(1 + c_t^{P(1)} g_0^2 + O(g_0^4)), \quad (2.10)$$

$$c_1 c_t^R(g_0^2) = c_1(3/2 + c_t^{R(1)} g_0^2 + O(g_0^4)), \quad (2.11)$$

where coefficients  $c_0$  and  $c_1$  of the improved gauge action are normalized such that  $c_0 + 8c_1 = 1$ . We call  $c_t^P(g_0^2)$  and  $c_t^R(g_0^2)$   $O(a)$  boundary improvement coefficients. So far, 1-loop coefficients  $c_t^{P(1)}$  and  $c_t^{R(1)}$  are independent each other. Weight factors  $W_i(\mathcal{C}, g_0^2)$ , which include loop corrections, becomes the Choice B of [11] in the weak coupling limit. The Choice B achieves the tree-level  $O(a)$  improvement and, at the same time, the lattice background field  $V$  in eq.(2.3) satisfies the equation of motion obtained by the variation of dynamical links.

Incidentally, we discuss the  $O(a)$  boundary counterterm from a different point of view. Here, it is assumed that the plaquette loops and rectangle loops which lie completely on the cylinder  $L^3 \times L$  are included in the action, and that each boundary consists of one time slice only. As explained in [1], at order  $a$  in the pure gauge theory, there are two possible boundary counterterms,  $a^4 \text{Tr}\{F_{0k}F_{0k}\}$  and  $a^4 \text{Tr}\{F_{kl}F_{kl}\}$ , each of which are summed over the  $x_0 = 0$  or  $x_0 = L$  hyper plane. Since the latter boundary term vanishes in the case of Abelian constant boundary field, in the following, we consider only the former. In this case, we have three candidates for  $O(a)$  boundary counterterms which respect lattice symmetries,

1. spatial sum of time-like plaquette loop that just touches one of the boundaries,
2. spatial sum of rectangle loop that has exactly 2 links on a boundary,
3. spatial sum of rectangle loop that has exactly 1 link on a boundary,

to satisfy one condition, the  $O(a)$  improvement condition. Therefore, for simplicity, we can take a trivial weight for the term 3, and we still have one degree of freedom for the choice of the boundary terms. At the tree level, however, the background field given in eq.(2.3) must satisfy the equation of motion<sup>1</sup>, so that one has to take  $c_t^P = 1$  and  $c_t^R = 3/2$  (Choice B). Since no such an extra constraint exists for the 1-loop boundary terms, we can freely set a relation between  $c_t^{P(1)}$  and  $c_t^{R(1)}$ , which will be given in the next section.

### 3 SF coupling and $O(a)$ boundary improvement coefficients

The SF with the improved gauge action is given by

$$\mathcal{Z} = e^{-\Gamma} = \int D[U] e^{-S[U]}, \quad (3.1)$$

---

<sup>1</sup>The equation of motion for the plaquette action is trivially satisfied.

where  $S[U] = S_{\text{imp}}[U]$ . We require the same boundary condition, eq.(2.2), for the link variables as in the case of the Wilson plaquette action. In perturbative calculations, there are two main concerns to note : one is whether the background field given by eq. (2.3) corresponds to the absolute minimum of the action, and the other is the gauge fixing. For the latter, we used the covariant gauge fixing procedure outlined in [1]. The former statement is positively proved in [1] for Wilson plaquette action. Unfortunately the statement has not been proved yet in the case of the improved gauge actions, since the proof in [1] is not applicable to these cases. In [9], however, it has been numerically checked that the background field given in eq. (2.3) corresponds to the minimum for a large class of improved actions, hence we assume this in our perturbative calculations.

In a neighborhood of the background field  $V$ , any link variables  $U$  can be parametrized by

$$U(x, \mu) = \exp\{g_0 a q_\mu(x)\} V(x, \mu), \quad (3.2)$$

where  $q_\mu$  are quantum fields. The SF coupling is defined through the free energy  $\Gamma$  in eq. (3.1)

$$\bar{g}_{\text{SF}}^2(L) = \frac{\Gamma'_0}{\Gamma'} \Big|_{\eta=\nu=0}, \quad (3.3)$$

where  $\Gamma'$  is the derivative with respect to  $\eta$ .  $\Gamma'_0$  is a normalization constant

$$\begin{aligned} \Gamma'_0 &= \frac{\partial}{\partial \eta} g_0^2 S[V] \Big|_{g_0^2=0} \\ &= \frac{\partial}{\partial \eta} \left[ c_0 \left\{ \sum_{P_t} 2\mathcal{L}(\mathcal{C}) + \sum_{P_{\text{other}}} 2\mathcal{L}(\mathcal{C}) \right\} + c_1 \left\{ \frac{3}{2} \sum_{R_t^2} 2\mathcal{L}(\mathcal{C}) + \sum_{R_{\text{other}}} 2\mathcal{L}(\mathcal{C}) \right\} \right] \Big|_{U=V} \\ &= 12 \left( \frac{L}{a} \right)^2 \left[ c_0 \left( \sin 2\gamma + \sin \gamma \right) + 4c_1 \left( \sin 4\gamma + \sin 2\gamma \right) \right], \end{aligned} \quad (3.4)$$

where  $\gamma$  is given in appendix A.

Let us discuss the perturbative expansion of the SF coupling. If we require that  $c_t^{P(1)}$  and  $c_t^{R(1)}$  satisfy (this is possible by using the last degree of freedom as mentioned in the end of the previous section)

$$c_t^{R(1)} = 2c_t^{P(1)}, \quad (3.5)$$

and introduce  $c_t^{(1)}$

$$c_t^{(1)} = c_0 c_t^{P(1)} + 4c_1 c_t^{R(1)} = c_t^{P(1)}, \quad (3.6)$$

then one obtains the relation between  $S[V]$  and  $\Gamma_0$

$$S[V] = \left( \frac{1}{g_0^2} + \frac{2a}{L} c_t^{(1)} \right) \Gamma_0 + O(g_0^2). \quad (3.7)$$

Using the eq.(3.7), the perturbative expansion of  $\bar{g}_{\text{SF}}^2(L)$  is given by

$$\bar{g}_{\text{SF}}^2(L) = g_0^2 + m_1^{(1)} (L/a) g_0^4 + O(g_0^6), \quad (3.8)$$

with

$$m_1^{(1)}(L/a) = -\frac{2a}{L}c_t^{(1)} + m_1^{(0)}(L/a), \quad (3.9)$$

where  $m_1^{(0)}(L/a)$  is the 1-loop correction to the SF coupling, calculated with the tree-level  $O(a)$  boundary coefficients, and the detail of the calculation will be given in the next section. The value of the 1-loop coefficient  $c_t^{(1)}$  is determined by the condition that the dominant part of the scaling violation of  $m_1^{(1)}(L/a)$  should be proportional to  $(a/L)^2$ , and then  $c_t^{P(1)}$  and  $c_t^{R(1)}$  are uniquely given by eq.(3.5) and eq.(3.6).

## 4 Calculation of the 1-loop coefficient

In the following, we choose lattice unit (i.e.  $a = 1$ ). According to the unpublished note [12], we have used  $I^a$  ( $a = 1, 2, \dots, 8$ ) as a basis of Lie algebra of SU(3) in the presence of the background field. Their explicit form can be found in [13]. Decomposing in a basis  $I^a$

$$q_\mu(x) = \sum_a \tilde{q}_\mu^a(x) I^a, \quad (4.1)$$

the quantum fields  $q_\mu$  are Fourier transformed with respect to spatial momenta as

$$\tilde{q}_0^a(x) = \frac{1}{L^3} \sum_{\mathbf{p}} e^{i\mathbf{p}\mathbf{x}} \tilde{q}_0^a(\mathbf{p}, x_0), \quad (4.2)$$

$$\tilde{q}_k^a(x) = \frac{1}{L^3} \sum_{\mathbf{p}} e^{i\mathbf{p}\mathbf{x}} e^{\frac{i}{2}(p_k + \phi_a(x_0))} \tilde{q}_k^a(\mathbf{p}, x_0), \quad (4.3)$$

where the phase  $\phi_a(x_0)$  is given in appendix A. In terms of  $\tilde{q}_\mu^a(x)$ , the quadratic part of the improved gauge action eq.(2.6) takes the form

$$S_{\text{imp}}^{(0)} = \frac{1}{L^3} \sum_{\mathbf{p}} \sum_{x_0, y_0=0}^{T-1} \sum_a \tilde{q}_\mu^a(-\mathbf{p}, x_0) K_{\mu\nu}^a(\mathbf{p}; x_0, y_0) \tilde{q}_\nu^a(\mathbf{p}, y_0), \quad (4.4)$$

with the condition

$$q_k(\mathbf{p}, x_0)|_{x_0=0} = 0, \quad \text{for } k = 1, 2, 3. \quad (4.5)$$

The explicit form of the inverse propagator  $K_{\mu\nu}^a$  is given in [11], and also in appendix A.

The 1-loop correction  $m_1^{(0)}(L)$  is given by

$$m_1^{(0)}(L) = -\frac{1}{\Gamma_0'} \frac{\partial}{\partial \eta} \left[ \frac{1}{2} \ln \text{Det} K - \ln \text{Det} \Delta_0 \right] \Big|_{\eta=\nu=0}, \quad (4.6)$$

where the determinant for the quantum field sector (the first term in the right hand side of the equation) is taken with respect to the spatial momentum  $\mathbf{p}$ , the time  $x_0$ , the Lie algebra sector  $a$  and Lorentz index  $\mu$ . The second term in the right hand of eq.(4.6) represents a contribution from the ghost sector. Here we will exclusively consider the quantum field sector, since the

contribution from the ghost sector to the 1-loop correction is same as in the case of Wilson plaquette action. Our boundary condition for the temporal component  $q_0$  is different from that in [1], so that the “non-uniform” contribution in the gauge fixing term remains in the inverse propagator  $K$  (see appendix A).

We evaluated the 1-loop correction  $m_1^{(0)}(L)$  numerically for the Iwasaki action ( $c_1 = -0.331$ ,  $c_2 = c_3 = 0$ ) [14], the Lüscher-Weisz (LW) action ( $c_1 = -1/12$ ,  $c_2 = c_3 = 0$ ) [15] and the DBW2 action ( $c_1 = -1.40686$ ,  $c_2 = c_3 = 0$ ) [16] in the range  $L = 6, \dots, 48$ . The results are shown in Table 1. The computations have been performed by using FORTRAN with the extended precision. As a check of our calculation, we have confirmed an independence of the gauge fixing parameter and expected symmetries before reducing the amount of the calculation [17]. We have also checked that our code at  $c_1 = 0$  reproduces the known result of the Wilson plaquette action [18]. Furthermore, two codes written independently by the two authors have produced identical results up to about 30 digits in the range  $L = 6, \dots, 32$ . Beyond this range, we have used the faster code only.

## 5 Analysis and results

In this section we extract the order  $1/L$  term from the 1-loop correction  $m_1^{(0)}(L)$  to determine the  $O(a)$  boundary improvement coefficient  $c_t^{(1)}$ . According to the Symanzik’s analysis of the cutoff dependence of Feynman diagrams on the lattice, one expects that 1-loop coefficient has an asymptotic expansion

$$m_1^{(0)}(L) \stackrel{L \rightarrow \infty}{\sim} \sum_{n=0}^{\infty} (A_n + B_n \ln L) / L^n. \quad (5.1)$$

Using the blocking method of [19], we extracted the first few coefficients  $A_0, B_0, A_1, B_1$  and estimated their errors.

Some of these coefficients are known or related to other quantities: For example,  $A_0$ ’s of two different actions are related to the ratio of  $\Lambda$ -parameters of two actions. If the ultra-violet divergences in the SF is removed by the standard renormalization of the coupling constant,  $B_0 = 2b_0$ , where  $b_0 = 11/(4\pi)^2$  is the 1-loop coefficient of the  $\beta$ -function in the pure SU(3) gauge theory. If the tree-level  $O(a)$  improvement is implemented,  $B_1 = 0$  must hold. Our main result comes from  $A_1$ : eq.(3.9) gives  $c_t^{(1)} = A_1/2$ .

We have first verified that our extraction of  $B_0$  and  $B_1$  is consistent with the above expectation. We have confirmed  $B_0 = 2b_0$  up to 7 digits(Iwasaki), 9 digits(LW) or 4 digits(DBW2), while  $B_1 < 10^{-4}$ (Iwasaki),  $< 10^{-7}$ (LW) or  $< 10^{-2}$ (DBW2). Since our data give expected values of  $B_0$  and  $B_1$ , we fix  $B_0 = 2b_0$  and  $B_1 = 0$  by hand, in the blocking procedure to extract  $A_0$  and  $A_1$ , whose results for each action are shown in Table 2 where we have added the result of plaquette action [8, 18] for a later reference.

As a further check, we extract  $A_0$ ’s from the ratio of  $\Lambda$ -parameters between two schemes  $X$  and  $Y$ , which is given by

$$\frac{\Lambda_X}{\Lambda_Y} = e^{-\frac{c}{2b_0}}, \quad (5.2)$$

$L$	Iwasaki action	LW action	DBW2 action
6	0.0865021015584032	0.3843092560841445	-0.2542597063902088
7	0.1026697312426737	0.4061279685078025	-0.2517151449619943
8	0.1171638577366678	0.4249279311929165	-0.2462340808659547
9	0.1303628849788211	0.4414718008748639	-0.2394316692834335
10	0.1424404981803593	0.4562496675217995	-0.2322864496797361
11	0.1535565273026473	0.4696045216347286	-0.2251762317750280
12	0.1638489264935022	0.4817875167578513	-0.2182314272034601
13	0.1734301653189940	0.4929883879248706	-0.2114993870451222
14	0.1823916642888328	0.5033540747374835	-0.2049961094379959
15	0.1908085280119190	0.5130007428050310	-0.1987234947986162
16	0.1987431354745856	0.5220218429952182	-0.1926766886112917
17	0.2062478088988484	0.5304936855855431	-0.1868475754585161
18	0.2133668331494581	0.5384793988419066	-0.1812265016307355
19	0.2201380038925787	0.5460318047790646	-0.1758031806343642
20	0.2265938267004754	0.5531955499144914	-0.1705672082184823
21	0.2327624550322364	0.5600087116401930	-0.1655083693982648
22	0.2386684311658198	0.5665040280450621	-0.1606168213494539
23	0.2443332770354413	0.5727098525006191	-0.1558831969805698
24	0.2497759696349747	0.5786509038428871	-0.1512986565129531
25	0.2550133267993803	0.5843488625662739	-0.1468549050440217
26	0.2600603227656853	0.5898228494962823	-0.1425441882890768
27	0.2649303482326239	0.5950898137064368	-0.1383592748238773
28	0.2696354261875951	0.6001648495876492	-0.1342934304660328
29	0.2741863922040979	0.6050614580595203	-0.1303403885609065
30	0.2785930459882241	0.6097917633368525	-0.1264943186395051
31	0.2828642794964034	0.6143666940320125	-0.1227497950252100
32	0.2870081858351735	0.6187961354134090	-0.1191017663623826
33	0.2910321522986861	0.6230890581649763	-0.1155455266354859
34	0.2949429402366960	0.6272536278701680	-0.1120766879801252
35	0.2987467539279429	0.6312972985837565	-0.1086911554135926
36	0.3024493002264770	0.6352268931891717	-0.1053851035018207
37	0.3060558404258739	0.6390486727199947	-0.1021549549113093
38	0.3095712355291510	0.6427683964162490	-0.0989973607544213
39	0.3129999859059953	0.6463913739632261	-0.0959091826148500
40	0.3163462661525911	0.6499225111032890	-0.0928874761305482
41	0.3196139558344332	0.6533663496047807	-0.0899294760096131
42	0.3228066666825220	0.6567271024057376	-0.0870325823576189
43	0.3259277667231945	0.6600086846150990	-0.0841943482007244
44	0.3289804017476282	0.6632147409439818	-0.0814124680962679
45	0.3319675144656546	0.6663486700493243	-0.0786847677306482
46	0.3348918616375112	0.6694136461978401	-0.0760091944125418
47	0.3377560294345988	0.6724126385966856	-0.0733838083775785
48	0.3405624472446620	0.6753484286860957	-0.0708067748282852

Table 1: 1-loop coefficient  $m_1^{(0)}(L)$  for improved actions.



where

$$\bar{g}_Y^2(\mu) = \bar{g}_X^2(\mu) + c\bar{g}_X^4(\mu) + \dots \quad (5.3)$$

A purely numerical number  $c$  here is given by

$$c = A_0^X - A_0^Y, \quad (5.4)$$

where  $A_0^X$  or  $A_0^Y$  is the expected  $A_0$  of the scheme  $X$  or  $Y$ , respectively. We then find

$$A_0^{\text{imp}} = A_0^{\text{plaq}} - 2b_0 \ln \left[ \frac{\Lambda_{\text{imp}}}{\Lambda_{\text{plaq}}} \right]. \quad (5.5)$$

Using  $A_0^{\text{plaq}} = 0.36828215(13)$  [8, 18] and the ratio of  $\Lambda$ -parameters <sup>2</sup>,

$$\frac{\Lambda_{\text{imp}}}{\Lambda_{\text{plaq}}} = \begin{cases} 59.05 \pm 1.0 & \text{for Iwasaki action [21]} \\ 5.29 \pm 0.01 & \text{for LW action [22]} \\ 1308 & \text{for DBW2 action [23]} \end{cases}, \quad (5.6)$$

we obtain the values of  $A_0^{\text{imp}}$  for each action, which are shown in Table 2 ( $A_0^{\text{exp}}$ ). We have observed the consistency in  $A_0$  between previous known results and our calculations.

With these confidences in our computation, we obtain the main result of our paper, the 1-loop  $O(a)$  boundary improvement coefficient eq.(3.9), which is given by

$$c_t^{(1)} = c_t^{P(1)} = A_1/2, \quad (5.7)$$

where  $A_1$  is also found in Table 2.

Finally, using our results  $A_0$  in Table 2, we can estimate the ratio of  $\Lambda$ -parameters between the improved action and the plaquette action more accurately,

$$\begin{aligned} \frac{\Lambda_{\text{imp}}}{\Lambda_{\text{plaq}}} &= \frac{\Lambda_{\text{imp}}/\Lambda_{\text{SF}}}{\Lambda_{\text{plaq}}/\Lambda_{\text{SF}}} = \exp \left\{ \frac{1}{2b_0} [A_0^{\text{plaq}} - A_0] \right\} \\ &= \begin{cases} 61.2064(3) & \text{for Iwasaki action} \\ 5.292104(5) & \text{for LW action} \\ 1273.4(8) & \text{for DBW2 action} \end{cases}. \end{aligned} \quad (5.8)$$

## 6 Conclusion and discussions

Combining our result of  $c_t^{(1)}$  for the improved gauge actions and the previous result of  $c_t^{(1)}$  for the clover quark action [7], we obtain

$$c_t^{P(1)} = c_t^{R(1)}/2 = A_1/2 + n_f c_t^{F(1)} \quad (6.1)$$

for the  $n_f$  flavors QCD, where  $c_t^{F(1)} = 0.0191410(1)$ .

<sup>2</sup>We take the value for DBW2 action from a private note [23].

As a final remark, let us discuss the lattice artifact of the step scaling function (SSF) [20] for various gauge actions. The SSF  $\sigma(s, u)$  describes the evolution of a renormalized coupling under finite rescaling factor  $s$  (say  $s = 2$ )

$$\sigma(s, u) = \bar{g}^2(sL) \Big|_{u=\bar{g}^2(L)}, \quad (6.2)$$

and it has a perturbative expansion

$$\sigma(s, u) = u + 2b_0 \ln(s)u^2 + O(u^3). \quad (6.3)$$

This SSF  $\sigma(s, u)$  in the continuum theory is obtained by the continuum limit of the lattice SSF  $\Sigma(s, u, 1/L)$ :

$$\sigma(s, u) = \lim_{1/L \rightarrow 0} \Sigma(s, u, 1/L). \quad (6.4)$$

Therefore we can estimate the lattice artifact of the SSF in our perturbative calculation. We define the relative deviation  $\delta(s, u, 1/L)$  and expand it as

$$\delta(2, u, 1/L) = \frac{\Sigma(2, u, 1/L) - \sigma(2, u)}{\sigma(2, u)} = \delta_1^{(k)}(2, 1/L)u + O(u^2), \quad (6.5)$$

where we have set that  $s = 2$  and  $\delta_1^{(k)}(2, 1/L)$  is the 1-loop coefficient. Here  $k$  denotes the degree of the improvement for the boundary coefficient: the tree (1-loop) value is used for  $k = 0$  ( $k = 1$ ).

The manifest form of  $\delta_1^{(k)}(2, 1/L)$  is given by

$$\delta_1^{(k)}(2, 1/L) = m_1^{(k)}(2L) - m_1^{(k)}(L) - 2b_0 \ln(2), \quad (6.6)$$

and the results, including data of the plaquette action [8, 18] for comparison<sup>3</sup>, are given in Table 3 for each gauge action. Figure 1 (Figure 2) shows that the 1-loop deviations with the tree-level (1-loop level)  $O(a)$  improved boundary coefficient vanish roughly linearly (quadratically) in  $1/L$  as expected. As is evident from Figure 1 and Figure 2, at 1-loop level, the lattice artifact for the renormalization group improved action (Iwasaki or DBW2) is comparable to or larger than that for the plaquette action, while the LW action is the least affected by the lattice cutoff. However, one can not conclude that the LW action is the best choice for numerical simulations, where the lattice artifacts of higher orders in  $u$  or  $a$  may not be negligible.

## Acknowledgements

S.T. would like to thank Dr. Saito for informative correspondence.

---

<sup>3</sup>We have added data for the plaquette action in the range  $L = 17, \dots, 24$

	plaquette action	Iwasaki action	LW action	DBW2 action
$A_0$	0.36828215(13)	-0.2049015(4)	0.136150567(6)	-0.62776(8)
$A_0^{\text{exp}}$		-0.1999(24)	0.13621(26)	-0.6159
$A_1$	-0.17800(10)	0.30360(26)	-0.005940(2)	0.896(45)

Table 2: The coefficients of asymptotic expansion  $A_0$ ,  $A_1$  for various gauge actions. The values for plaquette action are taken from [8, 18]

$L$	plaquette action		Iwasaki action		LW action		DBW2 action	
	$\delta_1^{(0)}$	$\delta_1^{(1)}$	$\delta_1^{(0)}$	$\delta_1^{(1)}$	$\delta_1^{(0)}$	$\delta_1^{(1)}$	$\delta_1^{(0)}$	$\delta_1^{(1)}$
6	0.01089	-0.00394	-0.01922	0.00608	0.000911	0.000417	-0.061	0.014
7	0.01004	-0.00268	-0.01684	0.00484	0.000659	0.000236	-0.050	0.014
8	0.00918	-0.00194	-0.01499	0.00399	0.000527	0.000156	-0.043	0.013
9	0.00841	-0.00148	-0.01356	0.00330	0.000441	0.000111	-0.038	0.011
10	0.00773	-0.00117	-0.01241	0.00277	0.000379	0.000082	-0.035	0.010
11	0.00714	-0.00095	-0.01146	0.00235	0.000333	0.000063	-0.032	0.009
12	0.00663	-0.00079	-0.01064	0.00201	0.000296	0.000049	-0.030	0.008
13	0.00618	-0.00066	-0.00994	0.00174	0.000268	0.000039	-0.028	0.007
14	0.00579	-0.00057	-0.00932	0.00152	0.000244	0.000032	-0.026	0.006
15	0.00544	-0.00049	-0.00878	0.00134	0.000224	0.000026	-0.024	0.006
16	0.00513	-0.00043	-0.00830	0.00119	0.000207	0.000022	-0.023	0.005
17	0.00486	-0.00038	-0.00787	0.00106	0.000193	0.000018	-0.022	0.005
18	0.00461	-0.00034	-0.00748	0.00095	0.000181	0.000016	-0.021	0.004
19	0.00438	-0.00030	-0.00713	0.00086	0.000170	0.000013	-0.020	0.004
20	0.00418	-0.00027	-0.00681	0.00078	0.000160	0.000012	-0.019	0.004
21	0.00399	-0.00025	-0.00652	0.00071	0.000151	0.000010	-0.018	0.003
22	0.00382	-0.00022	-0.00625	0.00065	0.000144	0.000009	-0.017	0.003
23	0.00367	-0.00020	-0.00601	0.00059	0.000137	0.000008	-0.017	0.003
24	0.00352	-0.00019	-0.00578	0.00054	0.000131	0.000007	-0.016	0.003

Table 3: The deviations for various gauge actions.

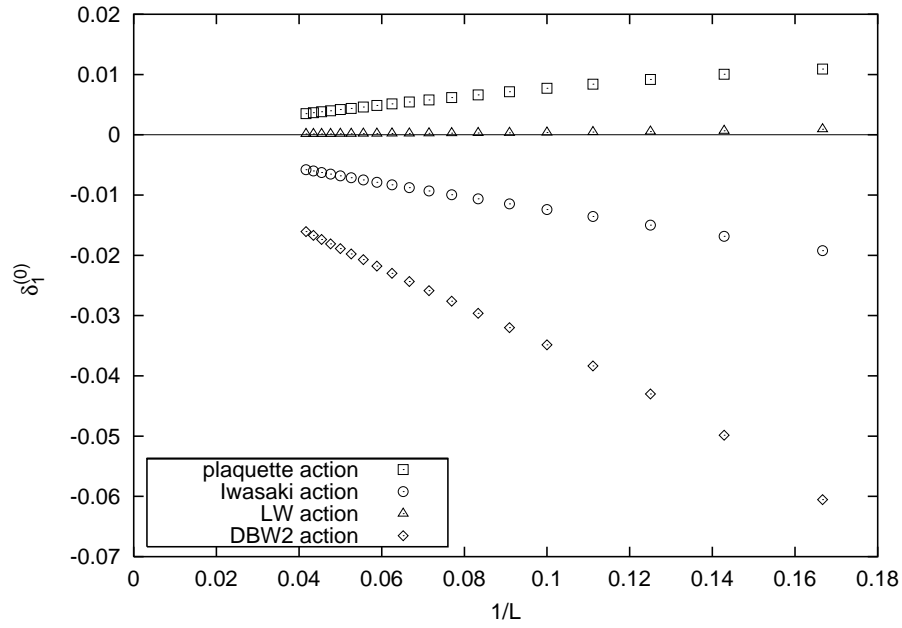


Figure 1: The relative deviations of the lattice SSF from the continuum one at 1-loop for various gauge actions with the tree-level  $O(a)$  improved boundary term. One can find that  $\delta_1^{(0)}$  for various gauge actions vanish roughly linearly in  $1/L$ .

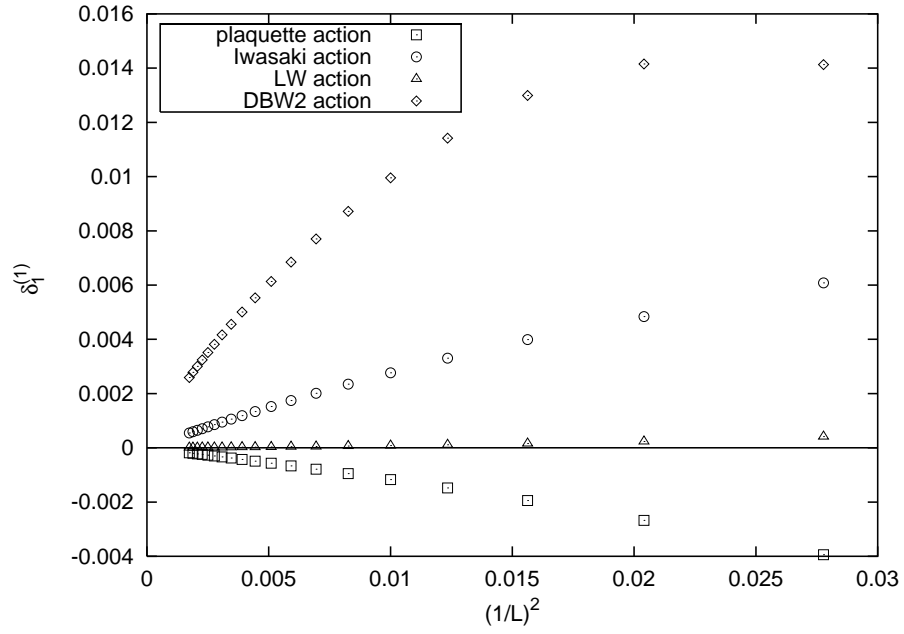


Figure 2: The same quantities as in Fig. 1, but with the 1-loop level  $O(a)$  improved boundary term. One can find that  $\delta_1^{(1)}$  for various gauge actions vanish roughly quadratically in  $1/L$ .

## A Inverse propagator

Here, we give the explicit form of the inverse propagator. We choose the lattice unit (i.e.  $a = 1$ ) and set  $T = L$ .

$$K = c_0 K^{(0)} + c_1 K^{(1)} + \lambda_0 K^{(\text{gf})}. \quad (\text{A.1})$$

### Plaquette

$$K_{00}^{(0)a}(\mathbf{p}; x_0, y_0) = R^a \delta_{x_0, y_0} \mathbf{s}^a(\mathbf{p}, x_0) \cdot \mathbf{s}^a(\mathbf{p}, x_0 + 1), \quad (\text{A.2})$$

$$K_{k0}^{(0)a}(\mathbf{p}; x_0, y_0) = iR^a \left[ \delta_{x_0, y_0} s_k^a(\mathbf{p}, x_0 + 1) - \delta_{x_0 - 1, y_0} s_k^a(\mathbf{p}, y_0) \right], \quad (\text{A.3})$$

$$K_{0k}^{(0)a}(\mathbf{p}; x_0, y_0) = -K_{k0}^{(0)a}(\mathbf{p}; y_0, x_0), \quad (\text{A.4})$$

$$K_{kl}^{(0)a}(\mathbf{p}; x_0, y_0) = \delta_{x_0, y_0} \left[ \delta_{kl} \mathbf{s}^a(\mathbf{p}, x_0)^2 - s_k^a(\mathbf{p}, x_0) s_l^a(\mathbf{p}, x_0) \right] + \delta_{kl} \left[ 2C^a \delta_{x_0, y_0} - R^a (\delta_{x_0 + 1, y_0} + \delta_{x_0 - 1, y_0}) \right]. \quad (\text{A.5})$$

### Rectangle

$w_{dbc} = 3/2$  for the choice B [11].

$$K_{00}^{(1)a}(\mathbf{p}; x_0, y_0)_{0kk} = \delta_{x_0, y_0} \left[ 1 + (w_{dbc} - 1)(\delta_{x_0, 0} + \delta_{x_0, L-1}) \right] \times 4R_2^a \sum_m \sin(\phi_a(x_0) + p_m) \sin(\phi_a(x_0 + 1) + p_m), \quad (\text{A.6})$$

$$K_{00}^{(1)a}(\mathbf{p}; x_0, y_0)_{00k} = R_2^a \sum_m \left\{ \delta_{x_0, y_0} \left[ (1 - \delta_{x_0, L-1}) s_m^a(\mathbf{p}, x_0) s_m^a(\mathbf{p}, x_0 + 2) \right. \right. \\ \left. \left. + (1 - \delta_{x_0, 0}) s_m^a(\mathbf{p}, x_0 - 1) s_m^a(\mathbf{p}, x_0 + 1) \right] \right. \\ \left. + \delta_{x_0 - 1, y_0} s_m^a(\mathbf{p}, x_0 - 1) s_m^a(\mathbf{p}, x_0 + 1) \right. \\ \left. + \delta_{x_0 + 1, y_0} s_m^a(\mathbf{p}, y_0 - 1) s_m^a(\mathbf{p}, y_0 + 1) \right\}, \quad (\text{A.7})$$

$$K_{k0}^{(1)a}(\mathbf{p}; x_0, y_0)_{0kk} = iR_2^a 2c_k^a(\mathbf{p}, x_0) \left[ \delta_{x_0, y_0} \{ 1 + (w_{dbc} - 1) \delta_{x_0, L-1} \} \sin(\phi_a(x_0 + 1) + p_k) \right. \\ \left. - \delta_{x_0 - 1, y_0} \{ 1 + (w_{dbc} - 1) \delta_{x_0, 1} \} \sin(\phi_a(y_0) + p_k) \right], \quad (\text{A.8})$$

$$K_{k0}^{(1)a}(\mathbf{p}; x_0, y_0)_{00k} = iR_2^a \left\{ s_k^a(\mathbf{p}, x_0 + 2) [(1 - \delta_{x_0, L-1}) \delta_{x_0, y_0} + \delta_{x_0 + 1, y_0}] \right.$$

$$-s_k^a(\mathbf{p}, x_0 - 2)[(1 - \delta_{x_0,1})\delta_{x_0-1,y_0} + \delta_{x_0-2,y_0}] \}, \quad (\text{A.9})$$

$$K_{0k}^{(1)a}(\mathbf{p}; x_0, y_0) = -K_{k0}^{(1)a}(\mathbf{p}; y_0, x_0), \quad (\text{A.10})$$

$$\begin{aligned} K_{kl}^{(1)a}(\mathbf{p}; x_0, y_0)_{0kk} &= \delta_{kl}c_k^a(\mathbf{p}, x_0)c_k^a(\mathbf{p}, y_0) \left[ 2C_2^a \delta_{x_0,y_0} - R_2^a(\delta_{x_0+1,y_0} + \delta_{x_0-1,y_0}) \right] \\ &+ (w_{abc} - 1)\delta_{kl}\delta_{x_0,y_0}c_k^a(\mathbf{p}, x_0) \left[ \delta_{x_0,1}(C_2^a c_k^a(\mathbf{p}, x_0) - iS_2^a s_k^a(\mathbf{p}, x_0)) \right. \\ &\quad \left. + \delta_{x_0,L-1}(C_2^a c_k^a(\mathbf{p}, x_0) + iS_2^a s_k^a(\mathbf{p}, x_0)) \right], \quad (\text{A.11}) \end{aligned}$$

$$\begin{aligned} K_{kl}^{(1)a}(\mathbf{p}; x_0, y_0)_{\text{others}} &= \delta_{x_0,y_0} \left[ \delta_{kl} \sum_m s_m^a(\mathbf{p}, x_0)^2 (c_k^a(\mathbf{p}, x_0)^2 + c_m^a(\mathbf{p}, x_0)^2) \right. \\ &\quad \left. - s_k^a(\mathbf{p}, x_0)s_l^a(\mathbf{p}, x_0)(c_k^a(\mathbf{p}, x_0)^2 + c_l^a(\mathbf{p}, x_0)^2) \right] \\ &+ \delta_{kl} \left[ (2 - \delta_{x_0,1} - \delta_{x_0,L-1})C_2^a \delta_{x_0,y_0} - R_2^a(\delta_{x_0+2,y_0} + \delta_{x_0-2,y_0}) \right]. \quad (\text{A.12}) \end{aligned}$$

## Gauge fixing term

$$\begin{aligned} K_{00}^{(\text{gf})a}(\mathbf{p}; x_0, y_0) &= 2\delta_{x_0,y_0} - \delta_{x_0+1,y_0} - \delta_{x_0-1,y_0} \\ &\quad - \delta_{x_0,y_0} [\delta_{x_0,0}(1 - \chi_a \delta_{\mathbf{p},\mathbf{0}}) + \delta_{x_0,L-1}], \quad (\text{A.13}) \end{aligned}$$

$$K_{k0}^{(\text{gf})a}(\mathbf{p}; x_0, y_0) = -is_k^a(\mathbf{p}, x_0)[\delta_{x_0,y_0} - \delta_{x_0-1,y_0}], \quad (\text{A.14})$$

$$K_{0k}^{(\text{gf})a}(\mathbf{p}; x_0, y_0) = -K_{k0}^{(\text{gf})a}(\mathbf{p}; y_0, x_0), \quad (\text{A.15})$$

$$K_{kl}^{(\text{gf})a}(\mathbf{p}; x_0, y_0) = \delta_{x_0,y_0} s_k^a(\mathbf{p}, x_0)s_l^a(\mathbf{p}, x_0). \quad (\text{A.16})$$

## Coefficients

$$s_k^a(\mathbf{p}, x_0) = 2 \sin[(p_k + \phi_a(x_0))/2], \quad (\text{A.17})$$

$$c_k^a(\mathbf{p}, x_0) = 2 \cos[(p_k + \phi_a(x_0))/2], \quad (\text{A.18})$$

$$\phi_a(x_0) = -\phi_{\bar{a}}(x_0), \quad (\text{A.19})$$

$$C^a = C^{\bar{a}}, \quad S^a = -S^{\bar{a}}, \quad R^a = R^{\bar{a}}, \quad (\text{A.20})$$

$$C_2^a = C_2^{\bar{a}}, \quad S_2^a = -S_2^{\bar{a}}, \quad R_2^a = R_2^{\bar{a}}, \quad (\text{A.21})$$

$$\chi_a = \chi_{\bar{a}} = (0, 0, 1, 0, 0, 0, 0, 1), \quad (\text{A.22})$$

$$\gamma = \frac{1}{L^2}(\eta + \frac{\pi}{3}), \quad (\text{A.23})$$

where  $\bar{1} = 2, \bar{4} = 5, \bar{6} = 7$ , and vice versa. For diagonal part,  $\bar{3} = 3, \bar{8} = 8$ .

### Lists of coefficients

$a$	$C^a$	$S^a$
1,4	$\frac{1}{2}(\cos 2\gamma + \cos \gamma)$	$-i\frac{1}{2}(\sin 2\gamma + \sin \gamma)$
3,6	$\cos \gamma$	0
8	$\frac{1}{3}(2 \cos 2\gamma + \cos \gamma)$	0

Table 4:  $C^a$  and  $S^a$  for SU(3).

$a$	$\phi_a(x_0)$	$R^a$
1	$-3\gamma x_0 + \frac{1}{L}(\eta[\frac{3}{2} - \nu] - \frac{\pi}{3})$	$\cos \frac{\gamma}{2}$
4	$-3\gamma x_0 + \frac{1}{L}(\eta[\frac{3}{2} + \nu] - \frac{2\pi}{3})$	$\cos \frac{\gamma}{2}$
3	0	$\cos \gamma$
6	$\frac{1}{L}(2\eta\nu - \frac{\pi}{3})$	$\cos \gamma$
8	0	$\frac{1}{3}(2 \cos 2\gamma + \cos \gamma)$

Table 5:  $\phi_a(x_0)$  and  $R^a$  for SU(3).

$a$	$R_2^a$	$C_2^a$	$S_2^a$
1,4	$\cos \gamma$	$R_2^a \cos 3\gamma$	$-iR_2^a \sin 3\gamma$
3,6	$\cos 2\gamma$	$R_2^a$	0
8	$\frac{1}{3}(2 \cos 4\gamma + \cos 2\gamma)$	$R_2^a$	0

Table 6:  $R_2^a, C_2^a$  and  $S_2^a$  for SU(3).



## References

- [1] M. Lüscher, R. Narayanan, P. Weisz and U. Wolff, Nucl. Phys. B384 (1992) 168
- [2] A. Bode et al. (ALPHA collaboration), Phys. Lett. B515 (2001) 49
- [3] M. Della Morte et al. (ALPHA collaboration), hep-lat/0209023
- [4] S. Aoki et al. (JLQCD collaboration), Nucl. Phys. Proc. Suppl. 106 (2002) 1079
- [5] S. Aoki et al. (JLQCD collaboration), Nucl. Phys. Proc. Suppl. 106 (2002) 263
- [6] S. Aoki et al. (CP-PACS collaboration), hep-lat/0211034
- [7] S. Sint, R. Sommer, Nucl. Phys. B465 (1996) 71
- [8] M. Lüscher, R. Sommer, P. Weisz and U. Wolff, Nucl. Phys. B413 (1994) 481
- [9] T. Klassen, Nucl.Phys. B509 (1998) 391
- [10] M. Lüscher, P. Weisz, Nucl. Phys. B240 (1984) 349
- [11] S. Aoki, R. Frezzotti, and P. Weisz, Nucl.Phys. B540 (1999) 501 and unpublished note.
- [12] P. Weisz,  $c_{sw}$  note (1996)
- [13] S. Kurth, PhD thesis, hep-lat/0211011
- [14] Y. Iwasaki, Nucl. Phys. B258 (1985) 141 ; Univ. of Tsukuba report UTHEP-118 (1983), unpublished.
- [15] M. Lüscher, P. Weisz, Commun. Math. Phys. 97 (1985) 59 : erratum-ibid.98 (1985) 433; Phys. Lett. 158B (1985) 250
- [16] T. Takaishi, Phys. Rev. D54 1050 (1996); P. de Forcrand et al., Nucl. Phys. B577 263(2000)
- [17] R. Narayanan, U. Wolff, Nucl. Phys. B444 (1995) 425
- [18] A. Bode, U. Wolff and P. Weisz, Nucl. Phys. B540 (1999) 491
- [19] M. Lüscher, P. Weisz, Nucl. Phys. B266 (1986) 309
- [20] M. Lüscher, P. Weisz and U. Wolff, Nucl. Phys. B359 (1991) 221
- [21] Y. Iwasaki, T. Yoshie, Phys. Lett. 143B (1984) 449
- [22] Y. Iwasaki, S. Sakai, Nucl. Phys. B248 (1984) 441
- [23] S. Sakai, T. Saito and A. Nakamura Nucl. Phys. B584 (2000) 528 ; private communication by Dr. Saito